

1 **Assessing the Global Resilience of Water Quality Sensor Placement Strategies**
2 **within Water Distribution Systems**

3 **Qingzhou Zhang¹, Feifei Zheng², Zoran Kapelan³, Dragan Savic⁴, Guilin He⁵, and Yiyi Ma⁶**

4 **¹Qingzhou Zhang:** Postdoctoral Research Fellow, College of Civil Engineering and
5 Architecture, Zhejiang University, China. wdswater@gmail.com.

6 **²Feifei Zheng:** Corresponding author, Professor, College of Civil Engineering and Architecture,
7 Zhejiang University, China. feifeizheng@zju.edu.cn. Tel: +86-571-8820-6757. Postal address:
8 A501, Anzhong Building, Zijingang Campus, Zhejiang University, 866 Yuhangtang Rd,
9 Hangzhou, China 310058.

10 **³Zoran Kapelan,** Professor, Delft University of Technology, Faculty of Civil Engineering and
11 Geosciences, Department of Water Management, Stevinweg 1, 2628 CN Delft, Netherlands.
12 z.kapelan@tudelft.nl

13 **⁴Dragan Savic:** Chief Executive Officer, KWR Water Research Institute,
14 Dragan.Savic@kwrwater.nl, Professor, Centre for Water Systems, University of Exeter, North
15 Park Road, Exeter, EX4 4QF, United Kingdom.

16 **⁵Guilin He:** Lectuer, School of Municipal and Environmental Engineering, Shandong Jianzhu
17 University, glhe@zju.edu.cn

18 **⁶Yiyi Ma:** Assistant Professor, College of Civil Engineering and Architecture, Zhejiang
19 University, China. yiyima@zju.edu.cn

20
21
22
23
24
25
26
27
28
29
30
31

32 **Abstract:** Water quality sensors are often spatially distributed in water distribution systems
33 (WDSs) to detect contamination events and monitor quality parameters (e.g., chlorine residual
34 levels), thereby ensuring safety of a WDS. The performance of a water quality sensor placement
35 strategy (WQSPS) is not only affected by sensor spatial deployment that has been extensively
36 analyzed in literature, but also by possible sensor failures that have been rarely explored so far.
37 However, enumerating all possible sensor failure scenarios is computationally infeasible for a
38 WQSPS with a large number of sensors. To this end, this paper proposes an evolutionary algorithm
39 (EA) based method to systematically and efficiently investigate the WQSPS' global resilience
40 considering sensor failures. First, new metrics are developed in the proposed method to assess the
41 global resilience of a WQSPS. This is followed by a proposal of an efficient optimization approach
42 based on an EA to identify the values of global resilience metrics. Finally, the sensors within the
43 WQSPS are ranked to identify their relative importance in maintaining the WQSPS's detection
44 performance. Two real-world WDSs with four WQSPSs for each case study are used to
45 demonstrate the utility of the proposed method. Results show that: (i) compared to the traditional
46 global resilience analysis method, the proposed EA-based approach identifies improved values of
47 global resilience metrics, (ii) the WQSPSs that deploy sensors close to large demand users are
48 overall more resilient in handling sensor failures relative to other design solutions, thus offering
49 important insight to facilitate the selection of WQSPSs, and (iii) sensor rankings based on the
50 global resilience can identify those sensors whose failure would significantly reduce the
51 WQSPS's performance thereby providing guidance to enable effective water quality sensor
52 management and maintenance.

53 **Keywords:** Global resilience; Contamination intrusion; Water quality sensor placement strategy;
54 Water distribution system

55 1. Introduction

56 A water distribution system (WDS) is a network that is responsible for delivering drinking water
57 produced at treatment plants to end users (Zheng et al., 2016; Qi et al., 2018). Because of a large
58 spatial coverage and complex structures, WDSs are highly vulnerable to intentional or accidental
59 contamination intrusion (Yang and Boccelli 2016; Zheng et al., 2018). A recent intrusion incident
60 was reported in May 2016 in Beijing, China, where a large amount of reclaimed water entered into
61 the WDS due to the misconnection between reclaimed and drinking water supply pipes
62 (ChinaNews, 2016). The event had not been detected for a while and has resulted in severe public
63 health hazard. This highlights the great importance and necessity to efficiently identify
64 contamination intrusion incidents, thereby minimizing the potential impacts of these events
65 (Ostfeld et al., 2004). To achieve this objective, water quality sensors are often placed within the
66 WDSs (i.e., type of sensors and their deployments) to form a contamination early warning system,
67 aimed to ensure potential intrusion events can be detected and a warning can be provided to the
68 public in an efficient manner (Wu and Walski, 2006; Hart and Murray, 2010; Kroll and King 2010;
69 Hu et al., 2017; Soldevila et al., 2018). However, due to the high cost associated with water quality
70 sensors, it is impossible to deploy them at all possible locations in a large WDS (Zhao et al., 2016).
71 This consequently motivates studies to investigate optimal deployment of a limited number of
72 sensors in the WDSs aimed at maximizing their performance in detecting water quality issues
73 (Rathi et al., 2015).

74 Identifying water quality sensor placement strategies (WQSPS) typically involves formulating an
75 optimization problem (Oliker and Ostfeld, 2014). Over the past decade, a number of different
76 optimization objective functions have been developed to maximize the detection ability of the
77 limited number of water quality sensors. These include the minimization of the detection time

78 (Ostfeld et al., 2004), the maximization of the detection coverage (Rathi et al., 2015), the
79 minimization of affected users (Aral et al., 2010), the minimization of sensor redundancy (Tinelli
80 et al., 2018), the minimization of the maximum possible influence expressed as the event with the
81 highest consequence (Watson et al., 2009), the minimization of the mean extent of the potential
82 source area and redundant detection (Van, 2014) as well as the minimization of the risk of
83 contamination (Weickgenannt et al 2010). It has been demonstrated that the use of different
84 objective functions can lead to significantly different WQSPSs, and hence it is often difficult to
85 identify a single WQSPS that can ensure all these objectives are optimized (Zheng et al., 2018). To
86 address this issue, the methods of integrating multiple objectives through weighting approaches or
87 simultaneously considering multiple objectives within the optimization framework are adopted to
88 account for the trade-offs between different objectives (He et al., 2018).

89 In parallel with the development of objective functions, many optimization techniques have been
90 proposed to enable these objective functions to be effectively minimized/maximized (Berry et al.,
91 2005; Bahadur et al., 2003; Hart and Murray, 2010). Among these optimization methods,
92 Evolutionary Algorithms (EAs) have gained in popularity due to their strong search ability as well
93 as their flexibility in linking to water quality simulation models (e.g., EPANET2.0, Ostfeld et al.,
94 2008). The practical applications of EAs to identify optimal WQSPSs are often challenged by their
95 low computational efficiency especially when dealing with large WDSs (Zheng et al., 2017). This
96 is because the EA search mechanisms are stochastically based and hence they need to call
97 continuously the water quality simulation model (that is often computationally expensive) to
98 enable the calculations of objective functions (Hart and Murray, 2010). To overcome this issue,
99 continuous efforts have been made to improve the optimization efficiency with the aid of many
100 techniques, including graph theory (Perelman and Ostfeld, 2011), preconditioning methods (Huang

101 and Mcbean, 2006; Diao and Rauch, 2013), surrogate models (Bi and Dandy, 2015), data-archive
102 methods (He et al., 2018) and sampling methods (Tinelli et al. 2017).

103 Given the selected objective function and the optimization algorithm as mentioned above, optimal
104 WQSPSs that have the best overall performance in detecting water quality issues can be identified
105 for the WDS. However, it should be noted that the WQSPS' performance is not only affected by
106 spatial sensor deployment, but can also be substantially influenced by sensor failures (e.g.,
107 structural failures and communication failures). Failures of water quality sensors are not
108 uncommon within practical applications, as they can be caused by internal structural failures,
109 measurement errors, or communication failures (Berry et al., 2009). These failures can
110 significantly reduce the performance of the optimal WQSPS that is identified based on the
111 assumption that all water quality sensors can consistently provide accurate measurements (Berry et
112 al., 2009). Therefore, there is a need to consider the resilience during the selection of WQSPSs,
113 thereby ensuring the system performs well not only under normal conditions (perfectly working
114 sensors), but also maintains acceptable functionality levels during unexpected conditions that lead
115 to sensor failures.

116 Resilience in engineering community is often defined as a system's ability to ensure the continuity
117 and efficiency of its function during and after the failure (Mugume et al., 2015). This concept has
118 now been considered in some engineering domains, such as urban drainage systems (Mugume et
119 al., 2015), water supply systems (Diao et al., 2016; Meng et al., 2018) and wastewater systems
120 (Sweetapple et al., 2019). However, to the best of our knowledge, the WQSPS's resilience that
121 accounts for sensor failures has been rarely investigated so far, and hence there is still a lack of
122 suitable method for resilience quantification. While Preis and Ostfeld (2008) and Berry et al.
123 (2009) have made attempts to consider sensor failures during the selection/assessment of WQSPSs,

124 they assume a known and fixed failure likelihood for each water quality sensor. However, these
125 approaches only considered a narrow range of possible sensor failures, and hence the results can
126 only represent a limited view of resilience (Mugume et al., 2015). Given that the failure
127 probability of each sensor as well as the total number of failed sensors is actually unknown and
128 unpredictable, it is ideal to explicitly consider all possible failure scenarios, thereby quantifying
129 the global resilience of the WQSPS in coping with possible sensor failures (Butler et al., 2014;
130 Diao et al., 2016). However, enumerating all possible sensor failure scenarios is often
131 computationally infeasible for WQSPSs with a large number of sensors. To this end, this study
132 proposes an EA-based method to investigate the global resilience of WQSPSs considering all
133 sensor failure scenarios.

134 Rather than quantifying the probability of occurrence of sensor failures, which are highly uncertain,
135 the proposed global resilience evaluation method considers the system performance as a result of
136 sensor failure scenarios irrespective of their occurrence probability (Diao et al., 2016). The
137 specific contributions/novelty of the present study are as follows:

- 138 (i) *The proposal of new metrics to assess the global resilience of WQSPSs under different*
139 *sensor failure levels (i.e., the number of failed sensors).* In this study, assessment metrics
140 are proposed to measure quantitatively the WQSPS's global resilience under different
141 sensor failure levels, where the impacts of different number of sensor failure scenarios on
142 the WQSPS's ability to detect contamination intrusions are considered, irrespective of their
143 occurrence probability.
- 144 (ii) *The development of a novel EA-based optimization approach to identify the values of the*
145 *global resilience metrics for different sensor failure levels.* To demonstrate the utility of the
146 proposed EA-based method (EAM), its performance is compared with the traditional global

147 resilience analysis (TGRA) approach (Diao et al., 2016) in capturing the impact extents of
148 the failure scenarios.

149 (iii) *Identification of the relative importance of the sensors in maintaining the WQSPS's*
150 *detection performance based on the global resilience metric values.* This also helps
151 improving knowledge of the underlying system properties of the WQSPSs as well as
152 offering important guidance for the management and maintenance of water quality sensor
153 systems.

154 This paper is organized as follows. The proposed methodology is described in Section 2, where the
155 definition of the global resilience metrics and the proposed EAM are presented. This is followed by
156 the descriptions of the case studies considered in Section 3, and results and discussions in Section 4.
157 Finally, the conclusion section (Section 5) shows the main observations and implications of this
158 paper.

159 **2. Methodology**

160 **2.1 Global resilience metrics for WQSPSs**

161 ***2.1.1 Global resilience metrics definition***

162 The proposed global resilience metrics are characterized by the consumed contaminated water of
163 the WDS during the contamination events. A more resilient WQSPS indicates its better ability in
164 detecting contamination events under different sensor failure levels and accordingly less
165 contaminated water would be consumed. The (percentage) functionality loss of the WQSPS under
166 different sensor failure levels (L) can be mathematically described as

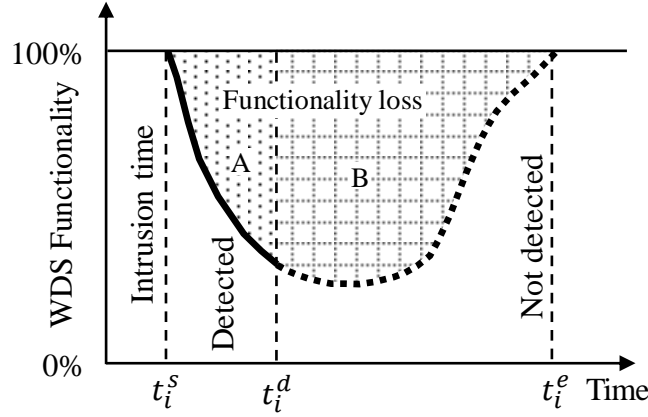
167
168
169
170
171
172
173
174
175
176
177
178
179
180
181
182
183
184
185

$$FL(S_L^k, E_i, t) = \frac{\sum_{j=1}^N Q_j(S_L^k, E_i, t)}{\sum_{j=1}^N DQ_j(t)} \quad (1)$$

where $FL(S_L^k, E_i, t)$ is the proportion of contaminated water that has been consumed relative to the total consumed water of the entire WDS under the intrusion event E_i ($i=1,2,\dots,M$, M is the total number of intrusion events) at time t for the sensor failure scenario k ($k=1,2,\dots,K$, K is the total number of sensor failure scenarios) with L failed sensors (referred as S_L^k); $Q_j(S_L^k, E_i, t)$ is the contaminated water that has been consumed at node j ($j=1,2,\dots,N$, N is the total number of nodes with demand users) and $DQ_j(t)$ is the total water demands required by node j .

Figure 1 further illustrates the proposed formulation of the global WQSPS resilience. As shown in this figure, the black solid curve line represents the dynamic behavior of the functionality level of the WDS (i.e., $1 - FL(S_L^k, E_i, t)$) associated with the WQSPS over time for a given contamination event E_i starting at time t_i^s and a given sensor failure scenario. It is seen that the functionality level of the WDS before the occurrence of the contamination event is 100%. This functionality level value consistently declines for the duration of the contamination event until this event is detected by the WQSPS within the WDS at time t_i^d . The shaded region A between t_i^s and t_i^d is the total functionality losses of the WDS (i.e., the consumed contaminated water) during this time period as indicated in Figure 1. If this contamination event cannot be detected by the WQSPS, the functionality level would gradually increase after a period of reduction as indicated by the black dotted line in Figure 1. This is because the contamination intrusion, especially the intentional contamination injections, often lasts a limited time period (e.g., 1 to 2 hours, see

186 Ostfeld et al., 2016 and He et al., 2018) and hence the functionality level of the WQS can
 187 improve as the contaminated water is consumed over time. For this case, the total functionality
 188 losses of the WDS are the shaded region A+B above the black solid and dotted curve lines in
 189 Figure 1.



190

191 **Fig. 1. Illustration of the dynamic behavior of the WDS's functionality level over time for a**
 192 **given contamination event and a given sensor failure scenario.**

193 For all M contamination events, the average of functionality levels (in percentage) of the WQSPS
 194 is developed as shown below

$$195 \quad f(S_L^k) = \frac{1}{M} \sum_{i=1}^M \left[1 - \frac{1}{(t_i^e - t_i^s)} \int_{t_i^s}^{T_i} FL(S_L^k, E_i, t) dt \right] \quad (2)$$

$$196 \quad T_i = \begin{cases} t_i^d, & E_i \text{ is detected} \\ t_i^e, & E_i \text{ can not be detected} \end{cases} \quad (3)$$

197 where $f(S_L^k)$ is the average of functionality levels (in percentage) of the WQSPS across M
 198 contamination events for the sensor failure scenario S_L^k ; $\int_{t_i^s}^{T_i} FL(S_L^k, E_i, t) dt$ is the accumulative

199 functionality losses for the intrusion event starting at time t_i^s and ending at time T_i , and this
 200 value is normalized between 0 and 1 through dividing it by the time difference between t_i^e and t_i^s
 201 (i.e., $t_i^e - t_i^s$), where t_i^e is the time at which all the contaminated water within the WDS has been
 202 consumed without detected by the water quality sensors. As shown in Equation (3), if a
 203 contamination event E_i can be detected by any sensors with normal functionalities, T_i equals to
 204 t_i^d which is the time at which any of the sensors first detects this event. If the contamination
 205 event cannot be detected, T_i is set to be t_i^e which is the time when all the contaminated water
 206 have been consumed by customers.

207 The rationale behind the use of the Equations (1) and (2) to represent the resilience of the
 208 WQSPS is that this formulation is able to simultaneously consider the impacts of sensor failures
 209 on the detection coverage and the time used to detect the contamination events, and the global
 210 resilience values are accordingly estimated when all possible failure scenarios are considered. In
 211 this study, three metrics are proposed to enable the global resilience assessment under a certain
 212 sensor failure level (L), which can be defined as follows

$$213 \quad R_{\max}(L) = \max \{f(\mathbf{S}_L)\} \quad (4)$$

$$214 \quad R_{\min}(L) = \min \{f(\mathbf{S}_L)\} \quad (5)$$

$$215 \quad R_{\text{mean}}(L) = \frac{1}{K} \sum f(\mathbf{S}_L) \quad (6)$$

216 where $R_{\min}(L)$, $R_{\max}(L)$, $R_{\text{mean}}(L)$ are the minimum, maximum and mean of global resilience
 217 values respectively for a given sensor failure level L ; $f(\mathbf{S}_L)$ is the performance level function

218 that is used to represent the resilience values of the WQSPSs and $\mathbf{S}_L = [S_L^1, S_L^2, \dots, S_L^K]^T$ is the set
219 that contains all possible scenarios with L failed sensors where K is the total number of sensor
220 failure scenarios; the resilience value of each scenario S_L^k is computed using Equation (1).

222 Based on the definition of the global resilience metrics in Equations (1-6), a more resilient WQSPS
223 would possess overall lower total functionality losses of the WDS (the shaded region in Figure 1)
224 when their sensors fail (considering different failure levels). It is noted that Figure 1 only illustrates
225 the dynamic behavior of the functionality level variations of the WDS over time for one
226 contamination event under a given sensor failure scenario. To enable the identification of the
227 global resilience, a large number of contamination events (M) and all possible sensor failure
228 scenarios (\mathbf{S}_L) need to be considered. The global resilience as proposed in this paper (Equations
229 1-6) can have a value between 0 and 1, with a larger value representing that the WQSPS being
230 considered is more resilient as it can maintain acceptable detection performance during
231 unexpected conditions that lead to sensor failures. Two important assumptions are made in the
232 proposed global resilience metrics following Ostfeld et al. (2008). These are that: (i) the
233 functionality level of the WDS is not further reduced once the contamination event has been
234 detected (the A shaded region in Figure 1) by the water quality sensors as all users can be
235 quickly notified/warned to avoid consuming contaminated water, and (ii) the time period of the
236 contamination injections is limited as this is often the case for many intentional/accidental
237 intrusion events (Diao et al., 2016).

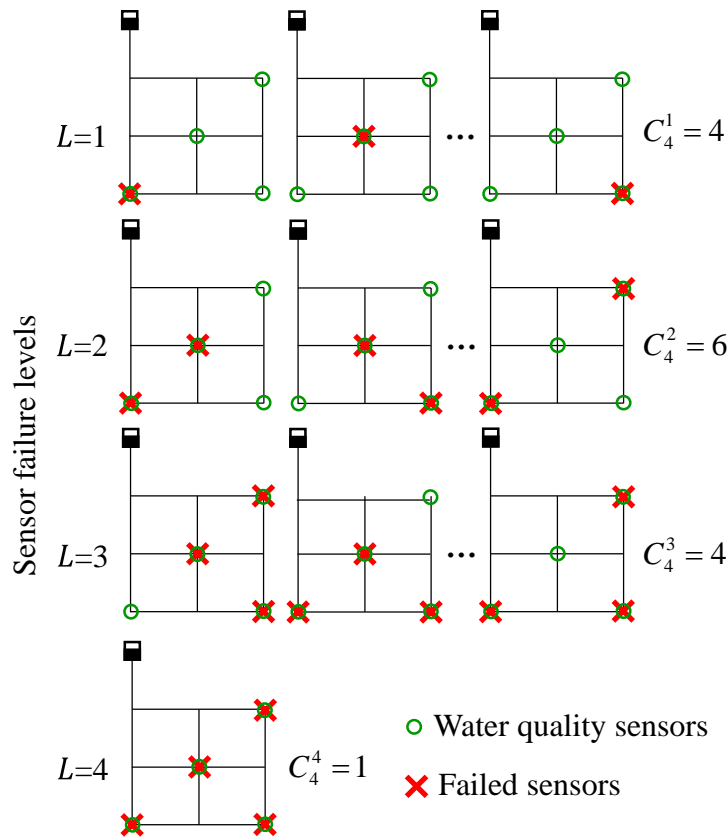
238

239

240

241 **2.1.2 Sensor failure scenarios**

242 As shown in Equations (4-6), S_L includes all possible failure scenarios for a given failure level L ,
 243 leading to a total of $C(TL, L)$ failure scenarios (TL is the total number of sensors within the
 244 WDS). Taking a WDS with four water quality sensors ($TL=4$) as an example, the total number of
 245 scenarios involving a random failure of a single sensor is four ($C(4,1) = 4$) as shown in Fig. 2.
 246 For failure levels of $L = 2, 3$ and 4, the total number of scenarios are six, four and one
 247 respectively (see Fig. 2). Therefore, for this small WQSPS, the total number of failure scenarios
 248 is 15.



249

250 **Fig. 2. A schematic of sensor failure scenarios in a simple WDS with four sensors at**
 251 **different failure levels (L). The total number of failure scenarios for $L=1, 2$ and 3 are $4, 6, 4$**

252 **respectively, but only three scenarios are given each of these three failure levels for**
253 **illustration purpose**

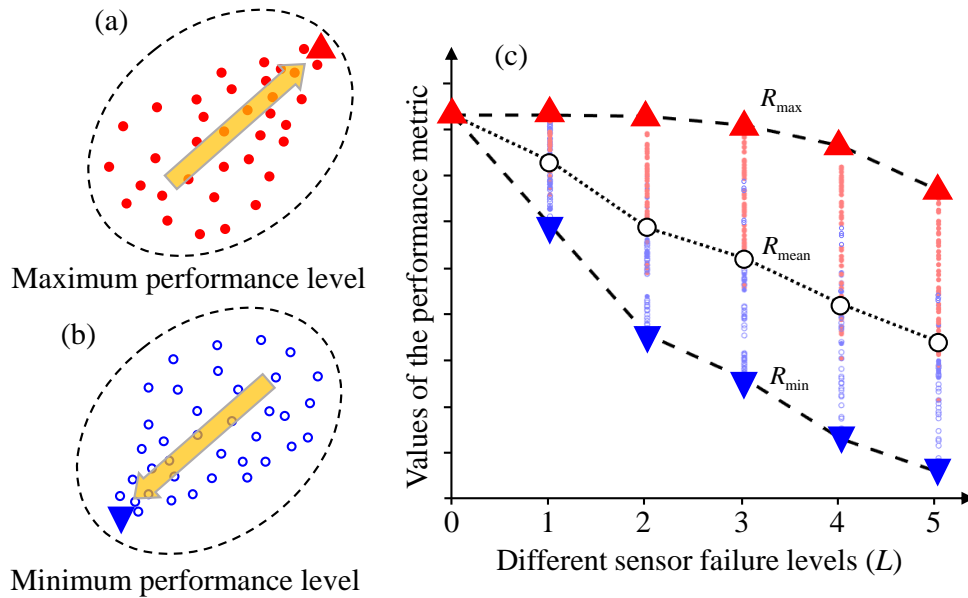
254 **2.2 Resilience Assessment using EA-based optimization**

255 *2.2.1 The EA-based method to identify global resilience values*

256 As stated in the previous section, for each failure level L , all possible failure scenarios have to be
257 considered to enable the computation of the global resilience metrics (See Equations 4-6).
258 However, enumerating all possible sensor failure scenarios is only applicable to WQSPS with a
259 small number of sensors. For a relatively large WQSPS this is not tractable. For example, if
260 WQSPS uses 30 sensors the total number of failure scenarios with $L = 1$ to 30 is 1.07×10^9 .
261 Simulating such a large number of scenarios requires massive computational resources, which
262 would significantly go beyond the computational budgets that are typically available in practice.
263 Therefore, the present study develops an efficient evolutionary algorithm based method (EAM) to
264 identify the global resilience metric values (Equations 4-6) for different sensor failure levels.

265 Figure 3 is used to illustrate the proposed EAM. For each given sensor failure level L , an EA is
266 performed to identify the sensor failure scenario that has the largest detection ability of the
267 remaining sensors of the WQSPS (Figure 3a), and the detection ability level is considered as the
268 global resilience value R_{\max} in Equation (4). More specifically, a large number of initial solutions
269 (sensor combinations with a given number of failed sensors L) are randomly generated, followed
270 by solution evaluations (Equations 1-3) with the aid of EPANET2.0 as the hydraulic and water
271 quality simulation model. These solutions are driven by the algorithm operations towards the
272 maximum value of the detection ability levels (Figure 3a) until the final optimal solution (i.e.,
273 R_{\max}) is identified (Wu and Walski, 2006). Similarly, the EA is run again to determine the sensor

274 failure scenario that has the lowest detection ability level of the remaining sensors of the WQSPS
 275 (Figure 3b), which is used to represent the global resilience value R_{\min} in Equation (5). All the
 276 individual members within the entire searching of the two optimization runs are used to estimate
 277 the mean value of the detection ability levels under sensor failures ($R_{\text{mean}}(L)$ in Equation 6), as
 278 shown in Fig. 3(c).



279
 280 **Fig. 3. Illustration of the proposed EA-based optimization method (EAM) to identify the**
 281 **global resilience values for different sensor failure levels (L)**

282 **2.2.2 The data-archive method to improve optimization efficiency**

283 In the proposed method, two EA optimization runs are performed for each sensor failure level,
 284 leading to a large number of EA runs as all different failure levels have to be considered. In
 285 addition, water quality simulation models need to be frequently called to enable the performance
 286 level computation (Equations 1-3) for each EA run, which are time-consuming especially for
 287 large-scale complex WDSs. To address this issue, a new data-archive method is developed in this

288 paper to improve the computational efficiency of the optimization process. The data-archive
289 method is based on the approach described in He et al. (2018)

290 In the proposed data-archive method, a calibrated water quality model is first established,
291 followed by the specification of simulation parameters such as simulation time step and duration
292 time. Subsequently, all possible contamination scenarios (intrusion events) are defined by adding
293 a contamination source with a given injection rate and a given time period to each node
294 $i = 1, 2, \dots, N$ at different time within the total duration of a simulation described by demand
295 patterns (DP). Therefore, the total number of contamination scenarios is $N \times DP$. A water
296 quality simulation is then executed with the pre-specified parameters for each pre-defined
297 intrusion event. A data-archive is finally established to record the hydraulic and water quality
298 simulation results that are required to enable the calculation of the performance levels as a result
299 of sensor failures. However, it should be noted that the proposed data-archive approach is used to
300 reduce the need for calling a water quality simulation model for each EA function evaluation
301 conditioned on a predefined set of contamination characteristics (e.g., intrusion concentration
302 and duration). This implies that the data archive needs to be re-developed if the intrusion
303 characteristics are changed. This is a limitation of the proposed data-archive approach that needs
304 to be addressed in future. The details of the proposed method for the development of data
305 archives are shown by the pseudo-code in Figure 4 below.

Step 0: Set up the water quality simulation model for the WDS.

Step 1: Specify the simulation parameters, including the water quality time step, contamination injection quantity, injection time period, concentration threshold and total simulation duration time.

Step 2: Define all the possible contamination intrusion events for each demand node $j = 1, 2, \dots, N$ (N is the total number of demand nodes) at time $t = t_1, t_2, \dots, t_{DP}$ (DP is the length of demand pattern) as $[E_1, E_2, \dots, E_M]$ ($M = N \times DP$).

FOR $i = 1, 2, \dots, M$

Step 3: Perform the water quality simulation with the pre-specified parameters for the intrusion event E_i (the start time of the injection and which node is to be injected)

```

FOR  $m=1,2,\dots,TL$  ( $TL$  is the total number of sensors)
  Step 4: Perform the water quality simulation model for the intrusion event  $E_i$  with the pre-
    specified total duration time
    If  $E_i$  can be detected by the  $m^{\text{th}}$  sensor
       $T_i = t_i^d$ 
    Otherwise
       $T_i = t_i^e$ 
  FOR  $t = 0, \Delta t, 2\Delta t, \dots, B\Delta t$  ( $T_i = B\Delta t$ )
    Step 5: Perform the water quality simulation model at time  $t$ , and record
       $Q_j(S_{TL-1}^m, E_i, t)$  and  $DQ_j(t)$  for each demand node  $j$ , where  $S_{TL-1}^m$  represents
      that only the  $m^{\text{th}}$  sensor is considered and the all the other sensors are failed
      (i.e., the failure level is  $TL-1$ ). This is followed by the use of Equation (1) to
      calculate and record  $FL(S_L^k, E_i, t)$  for each  $t$ .
    END  $t$ 
  Step 6: Compute  $\int_{t_i^s}^{T_i} FL(S_{TL-1}^m, E_i, t) dt$  in Equation (2), which equals to the total values of
     $FL(S_L^k, E_i, t)$  across different time.
  Step 7: Develop a data-archive for the event of  $E_i$  and the sensor  $m$ , referred to
     $\Phi(E_i, m) = \{t_i^s, t_i^e, T_i, \int_{t_i^s}^{T_i} FL(S_{TL-1}^m, E_i, t) dt\}$ 
  END  $m$ 
END  $i$ 

```

306 **Fig. 4. The pseudo-code of the development of the data archives in the proposed method**

307 Relative to the data-archive method stated in He et al. (2018) that only recorded the time of each
 308 sensor in detecting each of the contamination events (t_i^d), the archive structure used in this paper
 309 has been significantly extended by adding a larger number of variables including
 310 t_i^s, t_i^e, T_i , and $\int_{t_i^s}^{T_i} FL(S_{TL-1}^m, E_i, t) dt$ as shown in the pseudo-code (Figure 4). The application
 311 procedures of the developed data archives within the optimization framework are outlined in
 312 Figure 5 by pseudo codes. As shown in Figure 5, a total of Pop initial solutions is first randomly
 313 generated for each sensor failure level (L), followed by solution evaluations for all M intrusion
 314 events based on Equations 1-3. The individuals that are survived from the selection operator are

315 subject to cross and mutation operations, and the generated offspring are driven by the EA
 316 operations towards the optimal value until the final optimal solution is identified.

```

FOR  $L=1, 2, \dots, TL$ 
  FOR  $n=1, 2, \dots, Pop$  ( $Pop$  is the population size of the evolutionary algorithm, representing a
    sensor failure scenario with  $TL-L$  valid sensors)
    FOR  $i = 1, 2, \dots, M$  ( $M$  is the total number of intrusion events)
      Step 1: Identify the sensor  $m$  that has the minimum value of  $T_i$  information recorded
        at the data archive ( $\Phi$ ) from all  $TL-L$  valid sensors.
      Step 2: Compute and record  $\left[ 1 - \frac{1}{(t_i^e - t_i^s)} \int_{t_i^s}^{t_i^e} FL(S_L^k, E_i, t) dt \right]$  in Equation (2).
    END  $i$ 
      Step 3: Compute and record  $f(S_L^k)$  in Equation (2) using all the values recorded in
        Step 2.
    END  $n$ 
      Step 4: Carry out the algorithm operators to lead the search towards identifying the
        minimum or maximum resilience values as defined in Equations 4 and 5. All
        the recorded values in Step 3 over different EA iterations are used to
        compute the mean of the global resilience values in Equation (6).
  END  $L$ 

```

317 **Fig. 5. The pseudo-code of the applications of the data archives in the proposed method**

318 **2.3 Sensor Ranking**

319 In the proposed method, the sensors are ranked based on their impact on the global resilience
 320 values obtained using methodology shown in the above section, thereby indicating their relative
 321 importance in affecting the performance of the WQSPS induced by their failures. More
 322 specifically, the frequency of the sensors associated with the lowest global resilience values
 323 across different failure levels is used to enable the ranking, with details represented by the two
 324 equations below,

$$P_s(i) = \frac{1}{TL} \sum_{L=1}^{TL} \gamma(i, L) \quad (7)$$

$$\gamma(i, L) = \begin{cases} 1, & \text{Sensor } i \text{ is selected} \\ 0, & \text{Otherwise} \end{cases} \quad (8)$$

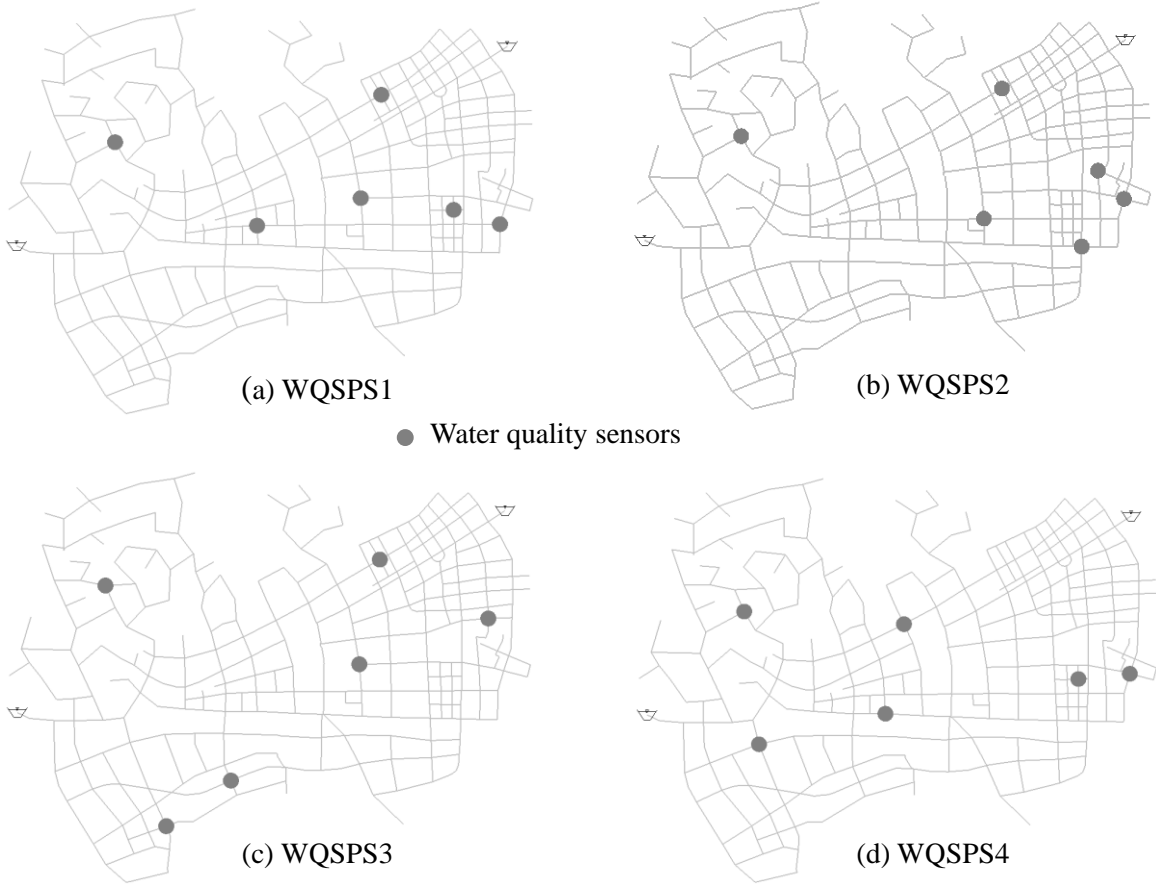
325 where $P_s(i)$ is the probability of the sensor i that has been identified to be included in the failure
 326 scenarios associated with the lowest reliance values (R_{\min}) over all different failure levels; TL is the
 327 total number of sensors; $\gamma(i, L)$ is an indicator function, with $\gamma(i, L) = 1$ if the sensor i is in the
 328 failure scenario of R_{\min} at the failure level L , which is identified by the EA-based optimization
 329 method, otherwise $\gamma(i, L) = 0$. For example, if a sensor is selected three times in the failure
 330 scenario of R_{\min} relative to a total of six failure levels, it has a $P_s(i) = 50\%$. As shown in Equation
 331 (7), a sensor with a larger value of $P_s(i)$ indicates that this sensor is overall more important as its
 332 failure is likely to induce more serious consequences relative to the sensors with low $P_s(i)$
 333 values. Such knowledge is practically important as it can be used as guidance for the
 334 management and maintenance of water quality sensor systems.

335 3. Case Studies

336 3.1. Description

337 Two real-world WDSs in China, the Jiayou network (JYN) and the Zhuohao network (ZHN), are
 338 selected as case studies to demonstrate the proposed EA-based global resilience assessment
 339 method. The JYN consists of two reservoirs, 349 demand nodes and 509 pipes with many loops
 340 (Figure 6), and The ZHN has one reservoir, 3,439 demand nodes and 3,512 pipes with many
 341 branches (Figure 7). Both WDSs have a demand pattern varying over 24 hours, with each hour

342 representing a demand scenario. The JYN and ZHN network supplies approximately 256,592 m³
343 per day and 140,782 m³ per day respectively. Six and 30 water quality sensors (He et al. 2018) are
344 available for JYN and ZHN, respectively. Four different water quality sensor placement
345 strategies (WQSPSs) have been identified for each case study as shown in Figures 6 and 7. These
346 four WQSPSs were identified by He et al. (2018) who used an optimization algorithm. Different
347 contamination probability functions were considered to enable the WQSPS optimization. More
348 specifically, the WQSPS1, WQSPS2, WQSPS3 and WQSPS4 for both case studies were
349 determined using the equal contamination probability function at each node, the probability
350 function based on nodal demands, the probability function based on length of pipes immediately
351 connected to the contaminated nodes, and the probability function based on user properties,
352 respectively (see He et al. (2018) for details). This study aims to investigate the global resilience
353 of the four WQSPSs with sensor failures considered, thereby facilitating the selection of the
354 resilient sensor deployment methods.

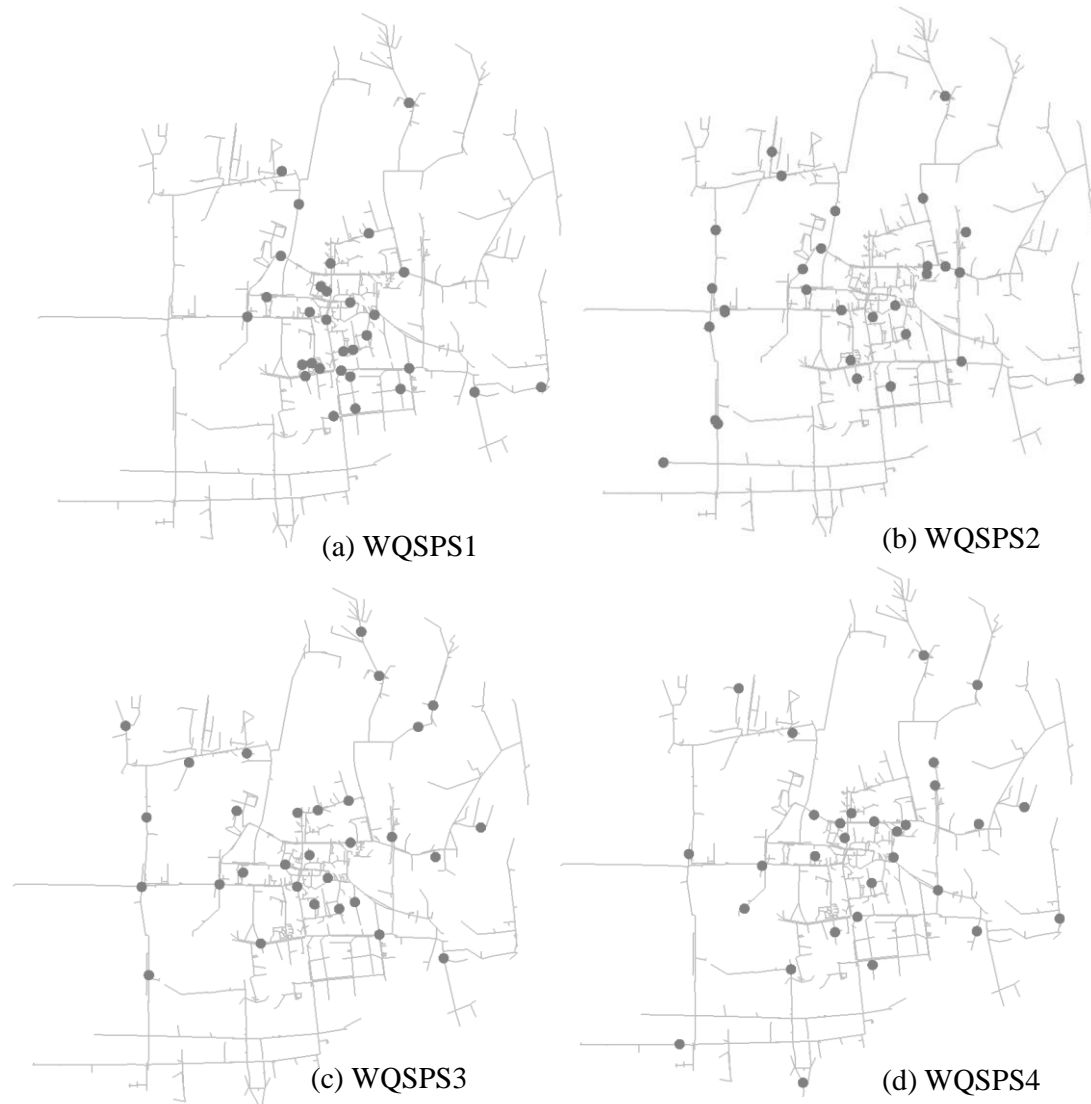


355

356 **Figure 6 The network typology of the JYN case study with four water quality sensor**

357

placement strategies (WQSPSs)



358

359 **Figure 7 The network typology of the ZHN case study with four water quality sensor**

360

placement strategies (WQSPSs)

361 *3.2 Application of the proposed method*

362 The EPANET2.0 was used as the hydraulic and water quality simulation model in this study. For

363 each case study, a total duration of 96 hours (four times of the 24-hour demand pattern) with a

364 time step of 5 minutes was used to simulate each contamination scenario. Following Ostfeld et al.

365 (2008), a contamination scenario was represented by adding a contamination source to a node

366 with an injection rate of 100 mg/L of two-hour duration. Consequently, the total numbers of
367 contamination scenarios for JYN and ZHN case studies were $24 \times 349 = 8,376$ and $24 \times 3439 =$
368 $82,536$, respectively. The detection threshold of water quality sensors was set to 0.01 mg/L
369 following He et al. (2018). It is noted that as each node of the WDS was considered as the
370 intrusion injection location at a wide range of injection time, it is believed that the defined
371 contamination events were representative following the description in Tinelli et al. (2017).

372 In the present study, the evolutionary algorithm Borg (Hadka and Reed, 2013; Zheng et al.,
373 2016), which has been successfully and widely used to deal with various water resources
374 optimization problems, was employed to solve the proposed optimization problem. The
375 population size of Borg applied to JYN and ZHN case studies were 500 and 1,000 respectively
376 following the parameters used in He et al. (2018), and the maximum allowable number of
377 evaluations was 500,000 for both case studies. The values of the remaining parameters of Borg
378 were the default selections in Wang et al. (2014), which have been validated and verified through
379 various applications. Five runs of the Borg with random number seeds were applied to each case
380 study, and the results were overall similar among different runs.

381 *3.3 The traditional global resilience analysis (TGRA) approach*

382 The traditional global resilience analysis (TGRA) approach has been widely used to assess the
383 resilience of various systems as a result of malfunctions (e.g., pipe breaks), such as electrical
384 power systems (Johansson, 2010), urban drainage systems (Mugume et al., 2015) and water
385 distribution systems (Diao et al., 2016). To demonstrate the capacity of the proposed EA-based
386 method, its performance is compared with the TGRA presented in Diao et al. (2016) in terms of
387 their ability to capture the global resilience values.

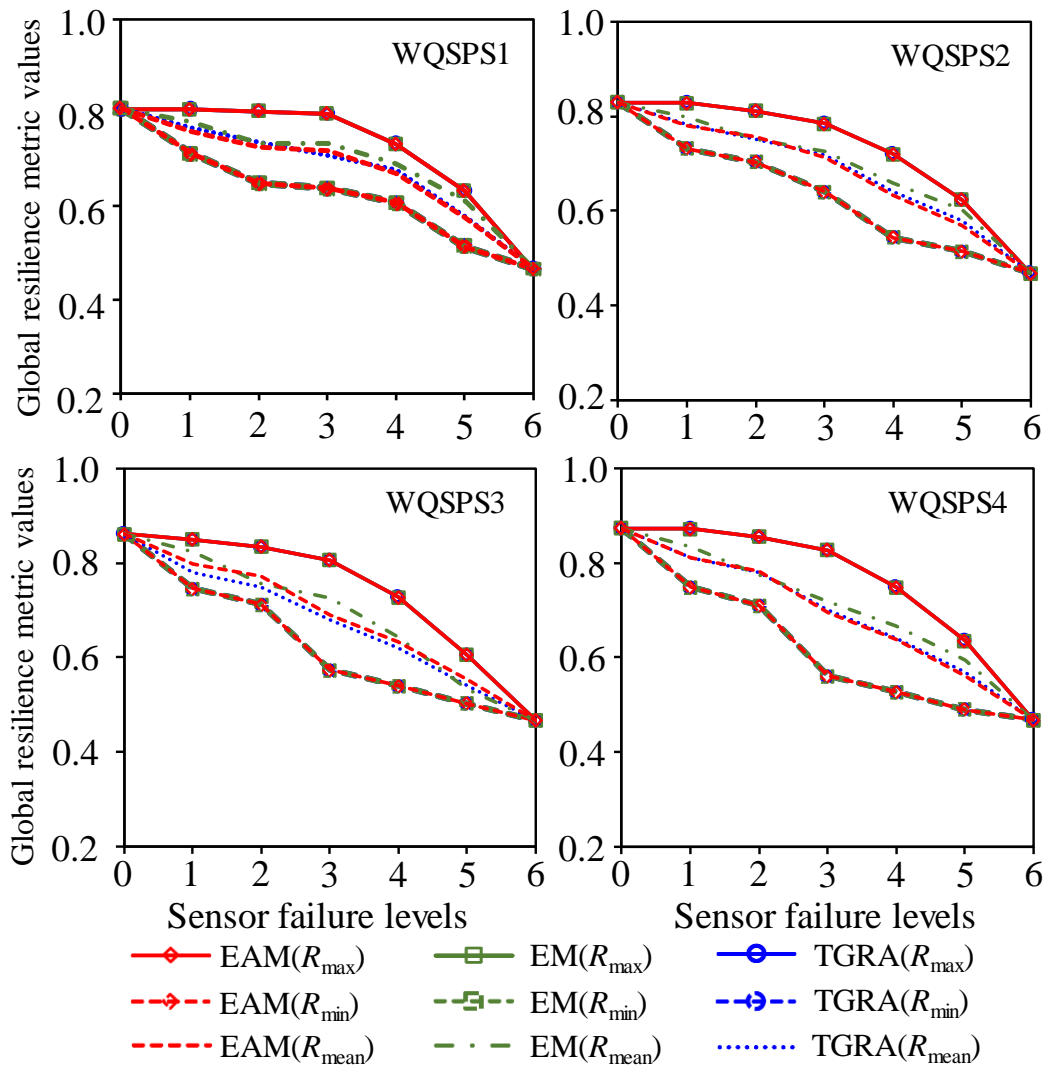
388 The TGRA provided a response curve (envelope) that represented the range of resilience
389 (corresponding Equations 4-6) under increasing failure levels by evaluating a limited number of
390 failure scenarios. When only one sensor in WDS failed (i.e., the failure level $L = 1$), it required
391 each sensor to be traversed and hence a total of M failure scenarios needed to be evaluated.
392 When all the sensors failed ($L = TL$), there was only one failure scenario to be considered. For
393 $1 < L < TL$, the TGRA involved two different types of failure scenario selections, which were
394 targeted failure type and random failure type (Diao et al., 2016). The targeted failure scenarios
395 were determined through an incremental manner, where the sensor with the largest/lowest impact
396 on the performance of WQSPS was incrementally added to the failure scenario as the failure
397 level increased. The random failure scenario selection aimed to enrich the targeted failure
398 scenarios through selecting the locations of L failed sensors randomly, thereby improving the
399 likelihood to identify the near-optimal failure scenarios that have the largest or lowest global
400 resilience values. Details of the TGRA can be found in Mugume et al. (2015) and Diao et al
401 (2016).

402 **4. Results and discussions**

403 *4.1 Comparison between the proposed EAM and the TGRA*

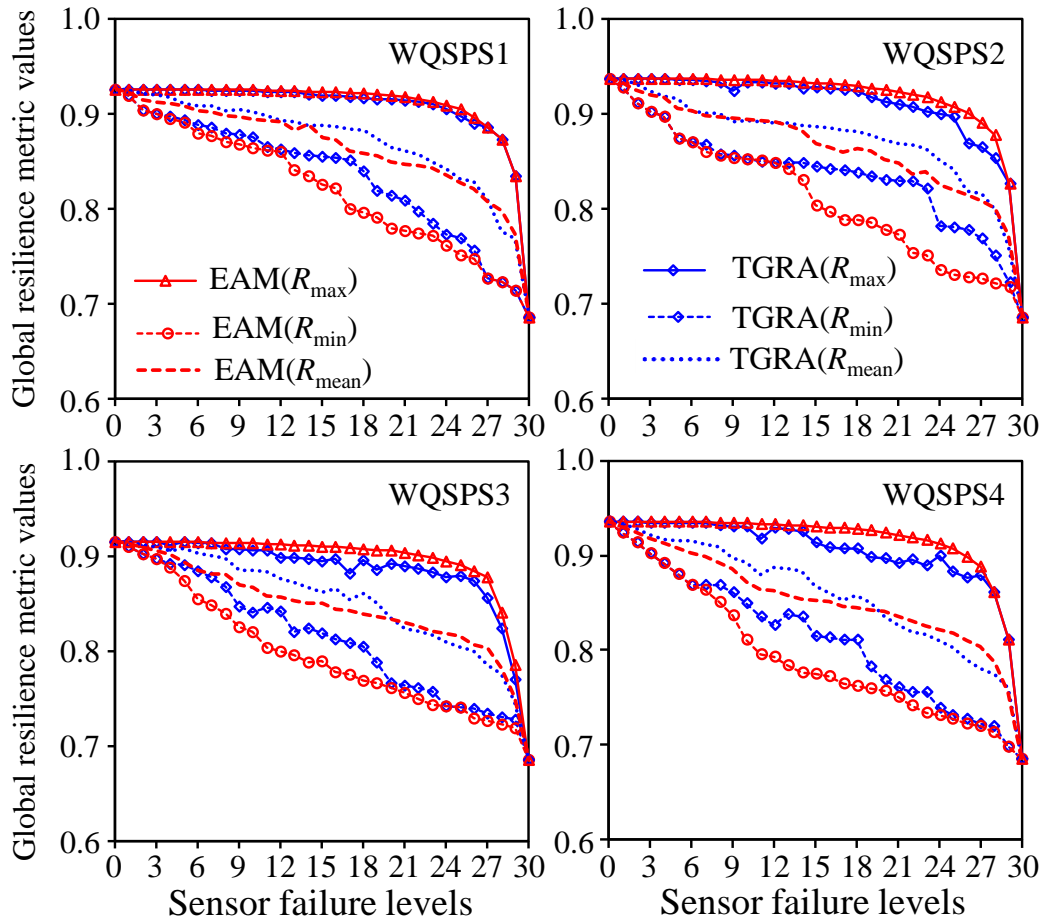
404 The values of the three global resilience metrics defined in Equations (4-6) were identified by the
405 proposed EAM and the TGRA respectively, with results given in Figures 8 (JYN) and 9 (ZHN).
406 For the JYN with a relatively small number of sensors (six), it was seen that the proposed EAM
407 exhibited similar performance with the TGRA in terms of R_{\max} , R_{\min} and R_{mean} values for each
408 failure level applied to the four sensor placement strategies (SPSs). To further verify the
409 effectiveness of the proposed EAM, all the possible failure scenarios for each failure level were

410 fully enumerated to enable the identification of the global values of the global resilience metrics,
 411 with results also shown in Figure 8 (the EM). It is observed that while the R_{mean} values were
 412 slightly different between the proposed EAM and the EM, the R_{max} and R_{min} values identified by
 413 the EAM consistently matched those from the EM. This was also the case for the traditional global
 414 resilience analysis method (TGRA) as shown in Figure 8. Using the results of the JYN case study
 415 with six sensors, it can be deduced that the proposed EAM was effective in identifying the global
 416 resilience values.



418 **Fig. 8. Global resilience metric values of different failure levels applied to the four different**
419 **WQSPSs of the JYN study**

420 Interestingly, when the methods were applied to the ZHN with 30 sensors (Figure 9), the
421 envelope results produced by the EAM results consistently outperformed those from the TGRA
422 across all sensor levels. This was especially the case for the R_{\min} as the proposed EAM was able
423 to identify sensor failure scenarios with substantially more serious impacts on the WQSPS's
424 detection performance compared to the TGRA. For instance, if 20 sensors failed for the SPS2
425 (Figure 9(b)), the value of R_{\min} identified by the proposed EAM was 0.78, but the TGRA offered
426 a value of $R_{\min}=0.84$. This indicated that the TGRA can significantly underestimate the potential
427 impacts of sensor failures on the detection performance of the water quality sensor systems. As
428 shown in Figure 9, the advantage of the proposed EAM relative to the TGRA became more
429 prominent for failure levels (L) between 10-20 (i.e., the number of failed sensors were between
430 10 and 20) for all the four WQSPSs. This was expected as the total search space for the L
431 between 10 and 20 was appreciably larger than other failure levels, and hence the TGRA had a
432 lower likelihood to identify the global resilience metric values (minimum or maximum values)
433 relative to the proposed EAM.

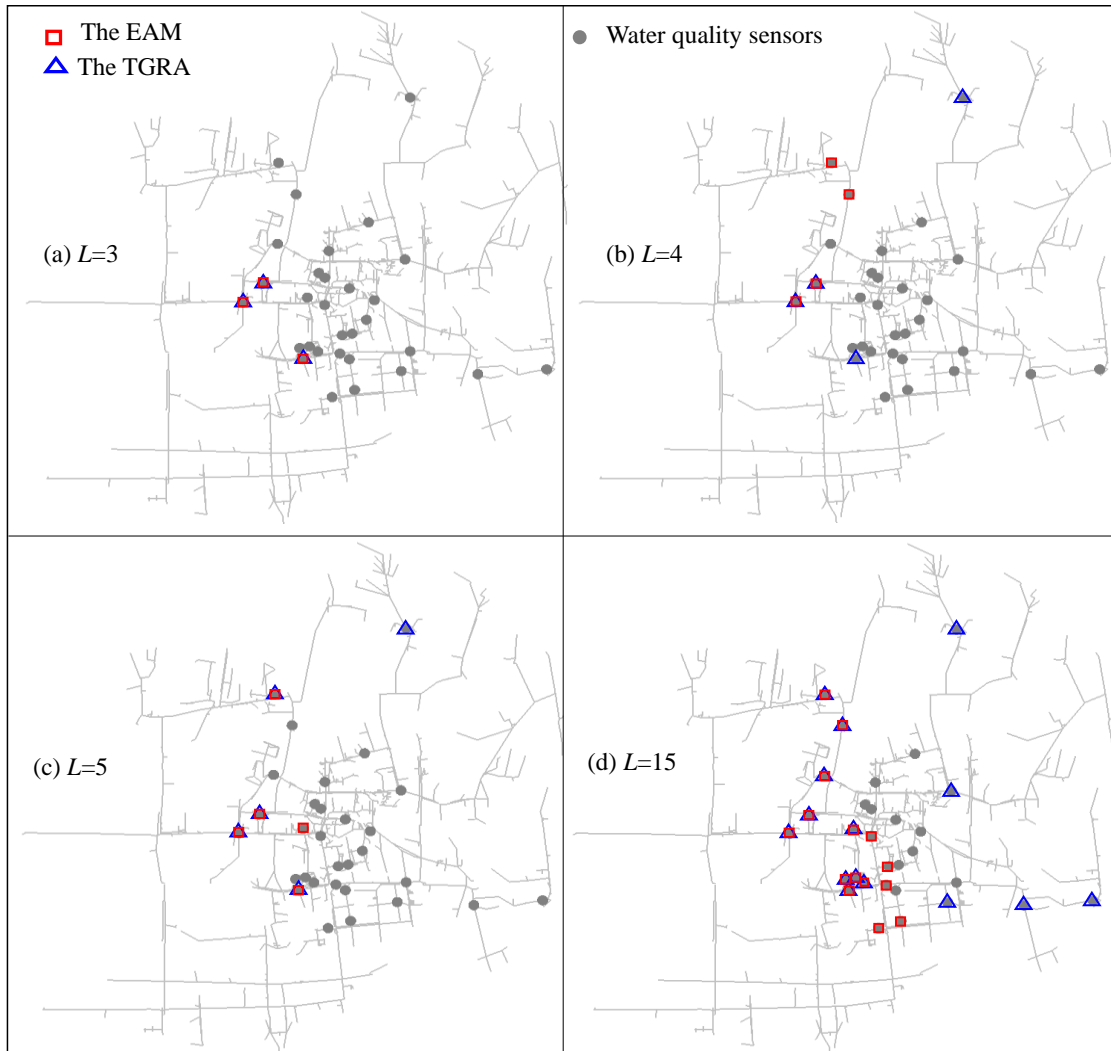


434

435 **Fig. 9. Global resilience metric values of different failure levels applied to the four different**
 436 **WQSPSs of the ZHN case study**

437 To reveal the underlying mechanisms that caused the performance variation between the
 438 proposed EAM and the TGRA, Figure 10 presents the locations of the failed sensors at four
 439 different failure levels (L) identified by these two methods applied to WQSPS1 of the ZHN case
 440 study based on R_{\min} metric. As shown in this figure, at $L = 3$, the locations of the three sensors
 441 with their failures having the largest impacts of the WQSPS1's detection performance were
 442 identical between these two methods (Figure 10a). However, for the EAM identified failure
 443 scenario based on R_{\min} metric when $L=4$ (Figure 10b), one sensor has been removed when

444 compared to the failure scenario with $L=3$, and two new sensors have been added to the failure
445 scenario with $L=4$. However, for the TGRA, only one more sensor has been added to its already
446 identified failure scenario based on R_{\min} metric when $L=4$. This was also the case when L
447 increased to 5 and 15 as shown in Figure 9(c,d). This was because the TGRA selected the failed
448 sensors mainly using an incremental (greedy) manner, where the sensor whose failure has the
449 largest impacts on the WQSPS's detection performance was incrementally added to the failure
450 scenario as the failure level increased. Therefore, the identified failed sensors were highly likely
451 to be trapped in a local solution. In contrast, the proposed EAM identified failed sensors
452 independently for each failure level, and hence it was able to find improved global resilience
453 metric values compared to the TGRA, especially for the large and complex problems (Figure 9).



454

455 **Fig. 10. Locations of sensors (to whose failure the resilience is sensitive) identified by the**
 456 **proposed EAM and TGRA methods applied to WQSPS1 (Figure 7) of the ZHN based on**

457

R_{\min} metric

458 In terms of computational analysis, the computational budgets of the proposed EAM were

459 primarily used by the generation of data archive that involved water quality simulations. For the

460 ZHN case study, the total number of contamination scenarios considered was the value computed

461 by the number of nodes (3,439) multiplied with the number of demand patterns (24), leading to a

462 total of 82,536 events. Using a PC with 4.00-GHz Intel Core i9-7980XE processor in Windows

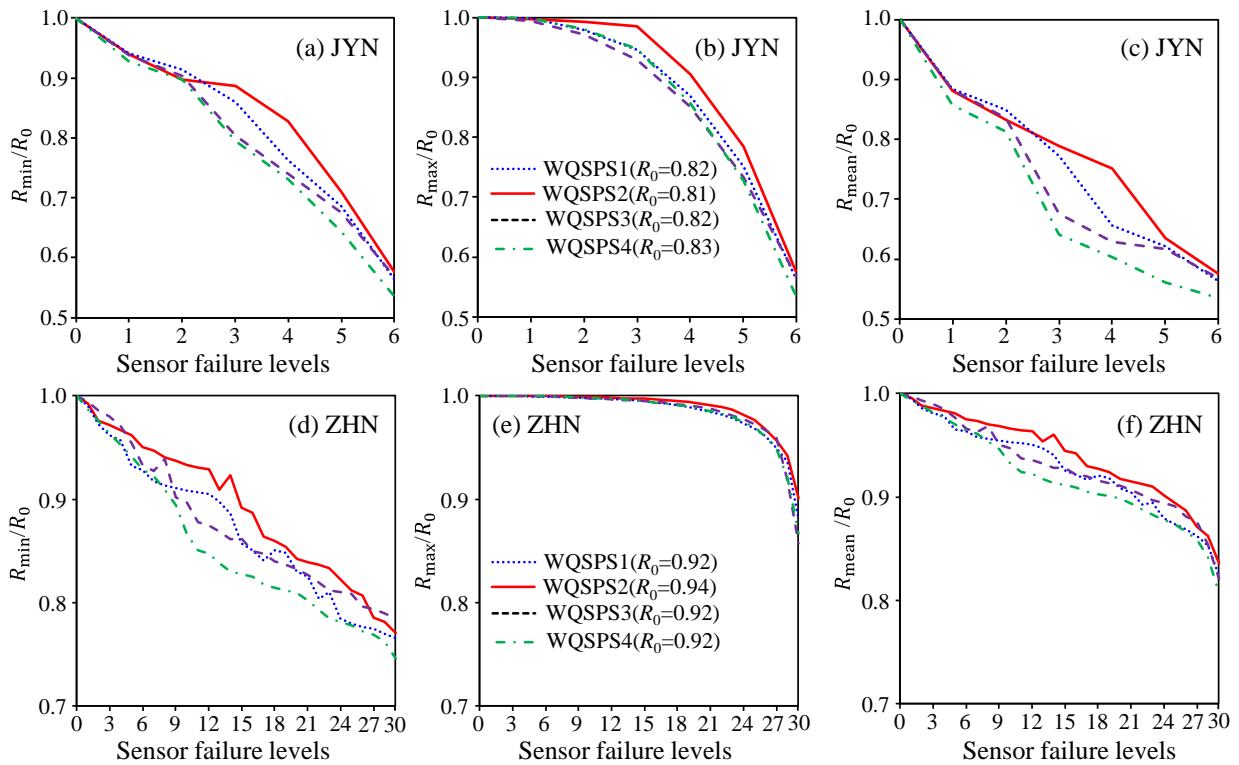
463 10, the total time for simulating these events for data archive development was 19.6 hours (note
464 that data archive only needed to be developed once). Within the optimization process, the
465 established data archive, rather than the water quality simulator, was used to enable the objective
466 function evaluations. Consequently, the optimization process was very efficient with a total of
467 approximately 0.5 hours for all optimization runs. Therefore, the total computational time used to
468 identify the global resilience metric values for the ZHN case study was 20.1 hours, which is
469 practically affordable. For the TGRA, a total of 11,679 sensor failure scenarios was identified
470 using the method described in Diao et al. (2016), and for each scenario, all the 82,536
471 contamination events had to be simulated to enable the objective function evaluations. The
472 estimated computational time was 229,261 hours or about 9,500 days ($11,679 \times 19.6$ hours used
473 for the simulating 82,536 contamination events), which is impossible to complete. Therefore, the
474 established data archive was also used by the TGRA to produce the results, and hence the total
475 computational time of the TGRA was similar to that used by the proposed EAM (the main
476 computational budgets of each method were used by the data archive establishment). This was
477 also the case for the small JYN case study. However, the proposed EAM can produce
478 significantly better results for the large ZHN case study compared to the TGRA as shown in
479 Figure 9.

480 4.2 Resilience comparison across different WQSPSs

481 Figure 11 shows the global resilience metric (R_{\min} , R_{\max} and R_{mean}) values of each WQSPS for the
482 two case studies over all different failure levels (L). All these values were divided by R_0 (the
483 global resilience value of WQSPS without sensor failures) to enable the performance comparison
484 of the four WQSPSs. As shown in Figure 11, for each case study, the R_0 values were overall

485 similar for the four WQSPSs, implying that the difference of the detection performance of the
 486 four WQSPSs without any sensor failures was negligible.

487 As expected, the detection performances of the four WQSPSs were consistently reduced as
 488 measured by the three global resilience metric values when the failure level increased for both
 489 case studies. Among the four WQSPSs, the WQSPS2 had an overall greater ability in
 490 maintaining its detection performance for both case studies under different failure levels
 491 compared to its counterparts. In contrast, the WQSPS4 exhibited the worst performance for the
 492 two case studies as it consistently exhibited the fastest performance deterioration in R_{\min} and
 493 R_{mean} induced by sensor failures with different levels.



494

495 **Fig. 11. Global resilience metric values of the four WQSPSs under all failure levels (L) for**

496 **the two case studies (R_0 is the global resilience value of WQSPS without sensor failures)**

497 The rationale behind the observations made above was that the WQSPS2 was identified based on
498 deploying sensors closer to large demand users (He et al. 2018). Therefore, the contamination
499 events at these large demand nodes that could result in large functionality losses of the WDS can
500 be detected in an efficient manner. Consequently, this sensor deployment strategy (WQSPS2)
501 tended to be overall more resilient as measured by the proposed global resilience metrics. While
502 the WQSPS4 also considered the demand values within its deployment, many sensors were
503 located exactly at the important users such as hospitals and schools as stated in He et al. (2018)
504 (this was the main difference between WQSPS2 and WQSPS4). Consequently, the global
505 resilience of this deployment strategy can be significantly reduced if the sensors at the important
506 users simultaneously failed. Therefore, the WQSPS2 was identified as the most resilient system
507 for both the JYN and ZHN case studies in dealing with sensor failures.

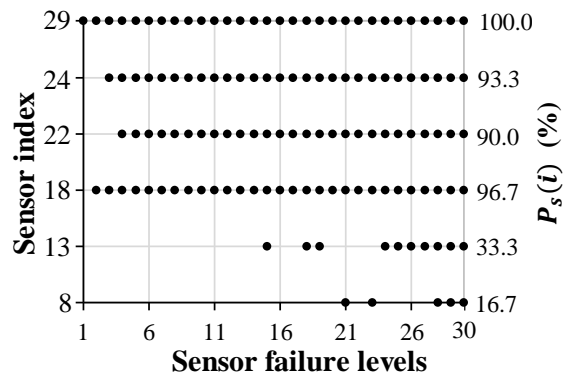
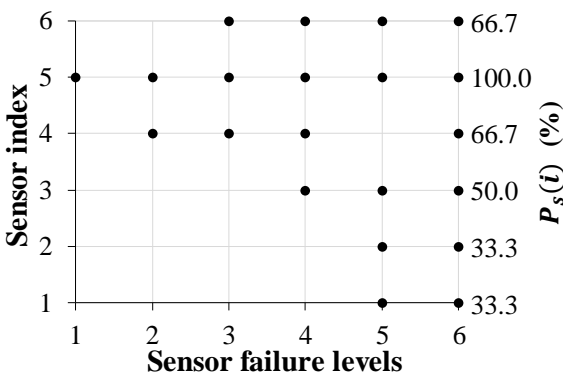
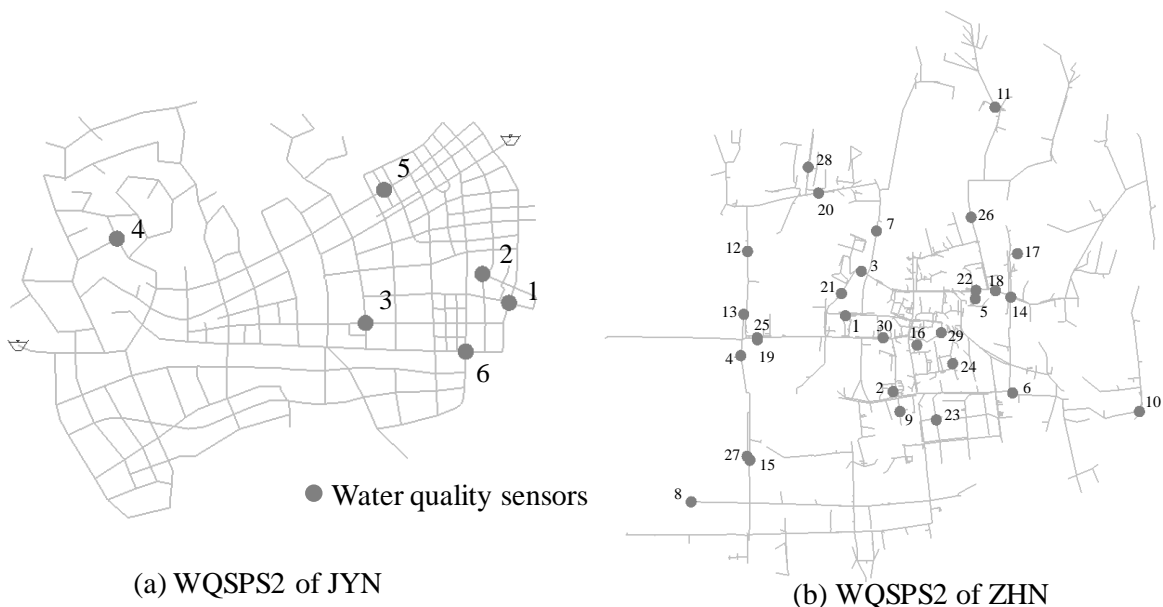
508 Another interesting observation from Figure 11 is that while WQSPS2 exhibited the overall best
509 performance in global resilience metric values across different failure levels, this sensor
510 deployment strategy performed similarly with the other three alternatives when the failure level
511 was low, such as L between 1 and 3. This is because many contamination events can be detected
512 by multiple sensors with relatively small time differences due to the looped water delivery
513 manner as well as relative large sensor density (e.g., 30 sensors for the ZHN). Consequently, the
514 relatively low sensor failure levels (e.g., $L=2$) would not induce significant variations across
515 different WQSPSs given that their initial detection ability levels were overall similar. This
516 implies that the global resilience that accounts for all possible failure scenarios (as it was done in
517 this study) can provide knowledge/insights, which goes beyond the resilience analysis only
518 considering limited failure scenarios (e.g., L between 1 and 3) as did in the majority of previous
519 studies (Preis and Ostfeld 2008, Berry et al. 2009).

520 4.3 Ranking the sensors within the WQSPSs

521 The sensors of the WQSPS2 for the JYN and the ZHN (identified as the most resilient design
522 solutions in the previous section) were ranked based on the R_{\min} values of all different failure
523 levels, with results given in Figure 12. It was seen that Sensor 5 was selected in all failure
524 scenarios (100% probability to be included in the failure scenarios) associated with R_{\min} within
525 the WQSPS2 of the JYN (Figure 12(c)), and hence this sensor was crucial in maintaining the
526 overall detection performance of the sensor system (the locations of Sensor 5 was shown in
527 Figure 12(a)). Sensor 4 was selected in addition to Sensor 5 as the two sensors that have the
528 largest impact on the WQSPS2 detection performance due to their simultaneous failures, i.e.,
529 $L=2$, as shown in Figure 12(c). For the WQSPS2 of the ZHN case study (ranks of only six
530 sensors were presented to enable clear visualization), Sensor 29 (Figure 12(b)) was the most
531 important sensor as it was consistently selected to be included in the failure scenarios that
532 produced R_{\min} (100% probability in Figure 12(d)). This was followed by Sensor 18 as it was
533 always selected from $L=2$ to 30 as shown in Figure 12(d). Detailed analysis of results revealed
534 that sensors with a relatively high rank were either located in the surrounding regions of the
535 large/important demand users or deployed in a region with sparse sensors. For example, Sensor 8
536 of the ZHN case study (low ranking with a relatively low probability) was only selected when L
537 was relatively large as shown in Figure 12(b,d). This was because this sensor was located at the
538 downstream end of the WDS and hence the impact of its failure on the WQSPS's detection
539 performance can be relatively small when compared to other sensors located in the middle of the
540 WDS.

541 The results of the sensor rankings based on the R_{\min} are practically significant as this knowledge
542 can be used as guidance to enable the effective water quality sensor maintenance management.

543 For instance, for the WQSPS2 of the JYN, Sensor 5 needed to be maintained more frequently
 544 than other sensors as its failure consistently resulted in larger performance reduction of the
 545 WQSPS over different failure levels. This was also the case for Sensor 29 within the WQSPS2 of
 546 the ZHN case study. From the practical point of view, the number of simultaneously failed
 547 sensors often ranged between 2 to 4, and for such cases, the ranking results obtained from the
 548 global resilience analysis can also inform the sensors whose failures have the largest impacts on
 549 the WQSPS's overall detection performance. For example, if $L=2$ was considered for the two
 550 case studies, Sensors 5 and 4 for the JYN and Sensors 29 and 19 for the ZHN were identified as
 551 the most important sensors that needed to be maintained in more frequently than other sensors.



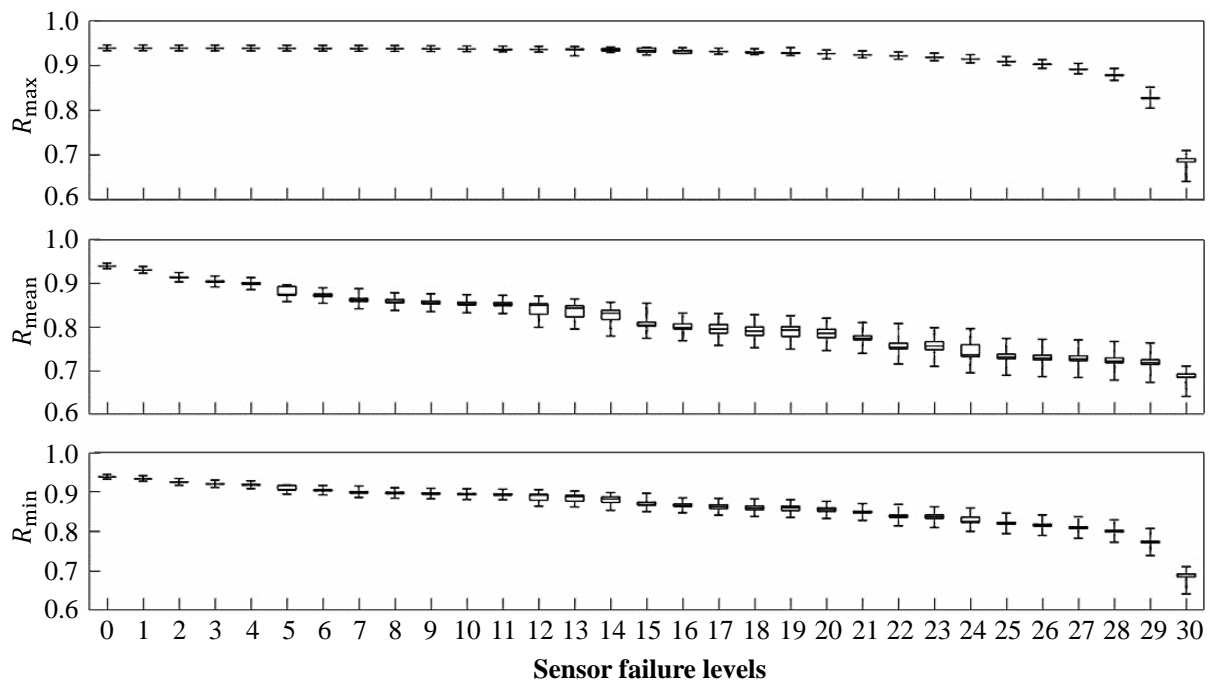
553 **Fig. 12. Sensor rankings based on the R_{\min} of all the failure levels for both case studies,**
554 **where $P_s(i)$ is the probability of the sensor i that has been identified to be included in the**
555 **failure scenarios associated with the lowest reliance values.**

556 *4.4 Sensitivity analysis*

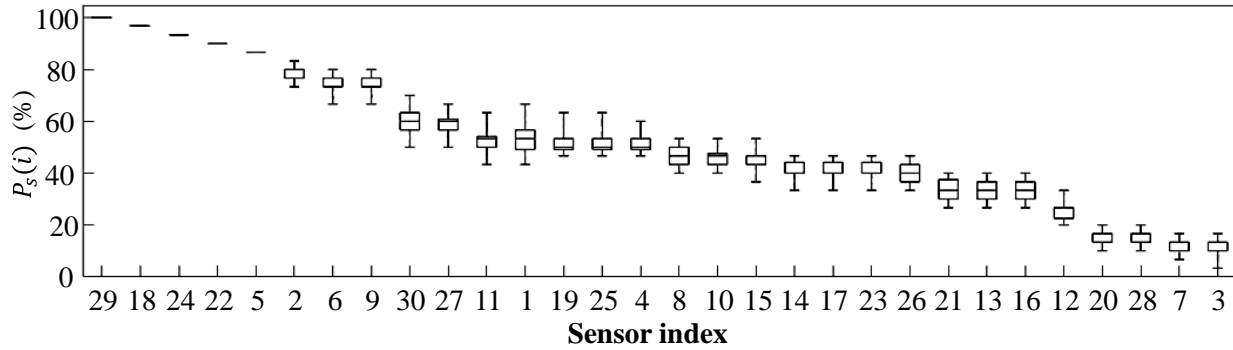
557 In this section, a sensitivity analysis was conducted to evaluate the impacts of the EA runs and
558 intrusion characteristics on the values of the global resilience metrics and sensor rankings. It is
559 noted that the parameters of the Borg were default values based on a comprehensive sensitivity
560 analysis performed in previous studies (Hadka and Reed, 2013; Zheng et al., 2016) and hence the
561 parameterization strategies of Borg were not explored in this paper. This is also partly because
562 Borg was only used as an optimization tool in the proposed method, rather than the research
563 focus of this study. Specifically, for each case study, five different invasion scenarios were
564 considered, which were 50 mg/L intrusion concentration with 1 hour duration, 100 mg/L
565 intrusion concentration with 1 hour duration, 100mg/L intrusion concentration with 2 hour
566 duration, 100 mg/L intrusion concentration with 3 hour duration, and 150 mg/L intrusion
567 concentration with 2 hour duration. For each invasion scenario, the proposed EA-based method
568 was run five times with different starting random seeds. Therefore, a total of 25 Borg runs were
569 performed invasion scenario, leading to 25 global resilience metric values (R_{\max} , R_{mean} and R_{\min})
570 and sensor rankings over all different failure levels.

571 Figure 13 presents the boxplot of global resilience metric values for the large ZHN case study
572 over all different failure levels. It can be observed from this figure that the variability of the
573 global resilience metric values was insignificant, which was especially the case for the relatively
574 low sensor failure levels. For instance, in terms of R_{\min} value, the largest variability occurred for

575 the sensor failure level $L=24$ with a maximum difference of 0.11 (from 0.69 to 0.80). Figure 14
 576 shows the boxplot of sensor rankings based on the R_{\min} values of all the failure levels calculated
 577 from the 25 solutions for the ZHN case study. As shown in this figure, the rankings of the
 578 sensors that were associated with a high probability $P_s(i) > 80\%$ were not affected by the choices
 579 of different invasion scenarios and starting random number seeds for Borg. However, for the
 580 sensors with a moderate value of $P_s(i)$ between 40% 60%, moderate variations were observed.
 581 Similar observations were made for the small JYN case study.



582
 583 **Fig. 13. Boxplot of global resilience metric (R_{\max} , R_{mean} and R_{\min}) values based on 25 Borg**
 584 **runs for the ZHN case study with five different invasion scenarios and five starting random**
 585 **number seeds over all different failure levels.**



586

587

Fig. 14. Boxplot of sensor rankings based on the R_{\min} of all the failure levels calculated

588

based on the 25 solutions for the ZHN case study, where $P_s(i)$ is the probability of the

589

sensor i that has been identified to be included in the failure scenarios associated with the

590

lowest reliance values

591

5. Summary and conclusions

592

A contamination early warning system is typically used to protect the water quality safety of a

593

water distribution system (WDS), where the water quality sensors are spatially distributed to

594

detect/warn contamination events. The majority of the current research focuses on identifying the

595

water quality sensor placement strategy (WQSPSs) based on an assumption that all sensors are

596

able to consistently provide accurate measurements, i.e., measure, record and communicate.

597

However, water quality sensors are generally vulnerable to their surrounding environment and

598

hence their failure likelihoods are often not insignificant. Therefore, it is critical to design a

599

resilient WQSPS that cannot only detect contamination events with great effectiveness when all

600

sensors are functioning normally, but also can maintain reasonable performance when sensors

601

fail. However, few attempts have been made so far to explore the WQSPS's resilience

602 considering sensor failures, especially for the global resilience that should account for all
603 possible failure scenarios.

604 This paper proposes a method to systematically assess the global resilience of WQSPSs with
605 sensor failures considered. In the proposed method, new metrics are firstly developed to represent
606 the global resilience of WQSPSs under different sensor failure levels (i.e., the number of
607 simultaneously failed sensors), where all possible sensor failure scenarios are considered
608 irrespective of their occurrence probability. Subsequently, an efficient Evolutionary Algorithm (EA)
609 based optimization approach is proposed to effectively identify the values of the global resilience
610 metrics for different sensor failure levels. Finally, the sensors within the WQSPS are ranked based
611 on their global resilience values. Two real-world WDSs with four WQSPSs for each WDS
612 analyzed are used to demonstrate the utility of the proposed global resilience identification method.
613 Based on the results obtained the following observations/implications can be made:

- 614 (i) The proposed EA-based optimization method (EAM) was able to identify improved
615 values of the global resilience metrics relative to the traditional global resilience analysis
616 (TGRA) method that has been widely used so far for the WDS with a large number of
617 sensors (Mugume et al., 2015, Diao et al., 2016). The advantage of the proposed EAM is
618 more prominent when dealing with WQSPSs with a large number of sensors. This
619 implied that the TGRA results may underestimate the potentially extreme
620 impacts/consequences of the sensor failures on the WQSPS's detection performance, and
621 this issue has been addressed using the proposed EAM.
- 622 (ii) It was observed that the WQSPSs designed based on deploying sensors relatively closer
623 to large demand users (WQSPS2) were overall more resilient in dealing with sensor
624 failures compared to other design solutions according to the definition of the global

625 resilience metrics (R_{mean}). However, the findings of this paper also showed that deploying
626 sensors very close to large users or important users (e.g., hospitals or schools) can also
627 risky as their failures can significantly reduce the detection performance of the WQSPS.
628 These insights were practically informative as it can be used to facilitate the selection of
629 WQSPSs for the WDS.

- 630 (iii) The sensor ranking based on the global resilience metric values (R_{min}) can identify the
631 important sensors whose failures would significantly reduce the WQSPS performance at
632 different failure levels. In addition, a sensitivity analysis showed that these rankings were
633 not significantly affected by the intrusion properties (injection concentrations and
634 durations). Such knowledge can provide guidance to enable efficient and effective water
635 quality sensor management as the highly ranked sensors were prioritized for maintenance
636 due to their large impacts on WQSPS's detection performance.

637 It should be noted that global resilience of identified optimal WQSPSs was assessed in the
638 current paper as suggested by previous studies (Mugume et al., 2015, Diao et al., 2016). This was
639 done post WQSPS optimization as incorporating such a methodology directly into the
640 optimization process would be extremely computationally expensive. It is acknowledged that
641 assessing the global resilience of WQSPS post-optimization rather than optimizing for global
642 resilience in the first place may result in sub-optimal solutions. Having said this, the proposed
643 method is still of high practical significance as the identification of sub-optimal solutions using
644 manageable computational efforts is often sufficient for real-world water resources problems
645 (Maier et al. 2014). Still, future studies should extend the proposed method to identify the most
646 resilient solutions considering sensor failures within the WQSPS design optimization process.

647 **Acknowledgement**

648 This work is funded by the National Natural Science Foundation of China (Grant No. 51922096),
649 and Excellent Youth Natural Science Foundation of Zhejiang Province, China (LR19E080003).

650 **References**

651 Aral, M.M., Guan, J.B., Maslia, M.L., 2010. Optimal design of sensor placement in water
652 distribution networks. *J. Water Resources Planning and Management* 136 (1), 5-18.

653 Bahadur, R., Samuels, W. B., Grayman, W., Amstutz, D., and Pickus, J. 2003. PipelineNet: A
654 model for monitoring introduced contaminants in a distribution system. Proc., World Water
655 and Environmental Resources Congress 2003 and Related Symp., ASCE, Reston, Va.

656 Berry, J., Carr, R. D., Hart, W. E., Leung, V. J., Phillips, C. A., and Watson, J. P. 2009. Designing
657 contamination warning systems for municipal water networks using imperfect sensors. *J.*
658 *Water Resources Planning and Management*, 135(4), 253–263.

659 Berry, J., Hart, W. E., Phillips, C. A., Uber, J. G., and Walski, T. M. 2005. Water quality sensor
660 placement in water networks with budget constraints. Proc., World Water and Environment
661 Resources Conf., ASCE, Reston, Va.

662 Bi, W., Dandy, G. C., & Maier, H. R. 2015. Improved genetic algorithm optimization of water
663 distribution system design by incorporating domain knowledge. *Environmental Modelling &*
664 *Software*, 69, 370-381.

665 Butler, D., Farmani, R., Fu, G., Ward, S., Diao, K., Astaraie-Imani, M. 2014. A new approach to
666 urban water management: Safe and SuRe. In: 16th Water Distribution System Analysis

667 Conference, WDSA. Procedia Engineering, pp. 347-354.
668 <http://dx.doi.org/10.1016/j.proeng.2014.11.198>.

669 ChinaNews, 2016. <http://www.chinanews.com/sh/2016/05-25/7883161.shtml>.

670 Diao, K., & Rauch, W. 2013. Controllability analysis as a pre-selection method for sensor
671 placement in water distribution systems. *Water research*, 47(16), 6097-6108.

672 Diao, K., C. Sweetapple, R. Farmani, G. Fu, S. Ward, and D. Butler. 2016. Global resilience
673 analysis of water distribution systems, *Water research*, 106, 383-393.

674 Hart W E and Murray. R. 2010, Review of sensor placement strategies for contamination warning
675 systems in drinking water distribution systems, *Journal of Water Resources Planning and*
676 *Management*, 136(6), 611-619.

677 Hadka, David and Patrick Reed. 2013. Borg: An Auto-Adaptive Many-Objective Evolutionary
678 Computing Framework. *Evolutionary Computation* 21, no. 2, 231-59.

679 He G, Zhang T, Zheng F, et al. 2018 An efficient multi-objective optimization method for water
680 quality sensor placement within water distribution systems considering contamination
681 probability variations. *Water research*, 143: 165-175.

682 Huang, J. J., McBean, E. A., & James, W. 2008. Multi-objective optimization for monitoring
683 sensor placement in water distribution systems. In *Water Distribution Systems Analysis*
684 *Symposium 2006* (pp. 1-14).

685 Hu, C., Ren, G., Liu, C., Li, M., Jie, W. 2017. A spark-based genetic algorithm for sensor
686 placement in large scale drinking water distribution systems. *Cluster Computing*. 20 (3), 1-11.

687 Johansson, J., 2010. Risk and Vulnerability Analysis of Interdependent Technical Infrastructures
688 Addressing Socio-technical Systems (PhD thesis). Lund University, Lund.

689 Kroll and King. 2010 Methods for evaluating water distribution network early warning systems.
690 Journal: American Water Works Association, 102(1), 1-11.

691 Maier, H. R., Kapelan, Z., Kasprzyk, J., Kollat, J., Matott, L. S., Cunha, M. C., Dandy, G. C.,
692 Gibbs, M. S., Keedwell, E., Marchi, A., Ostfeld, A., Savic, D., Solomatine, D. P., Vrugt, J.
693 A., Zecchin, A. C., Minsker, B. S., Barbour, E. J., Kuczera, G., Pasha, F., Castelletti, A.,
694 Giuliani, M., and Reed, P. M. (2014). "Evolutionary algorithms and other metaheuristics in
695 water resources: Current status, research challenges and future directions." *Environmental*
696 *Modelling & Software*, 62(0), 271-299.

697 Meng, F., G. Fu, R. Farmani, C. Sweetapple, and D. Butler. 2018, Topological attributes of
698 network resilience: A study in water distribution systems, *Water research*, 143, 376-386.

699 Mugume S N, G. D. E., Fu G, et al. 2015, A global analysis approach for investigating structural
700 resilience in urban drainage systems, *Water research*, 81, 15-26.

701 Olikier N, Ostfeld A. 2014. A coupled classification–evolutionary optimization model for
702 contamination event detection in water distribution systems. *Water research*, 51, 234-245.

703 Ostfeld, A., and Salomons, E. 2004. Optimal Layout of Early Warning Detection Stations for
704 Water Distribution Systems Security. *Journal of Water Resources Planning & Management*,
705 130(5), 377-385.

706 Ostfeld, A. et al. 2008 "The battle of the water sensor networks (BWSN): A design challenge for
707 engineers and algorithms." *Journal of Water Resources Planning and Management* 134(6),
708 556-568.

709 Perelman, L., Ostfeld, A. 2011. Extreme impact contamination events sampling for real-sized
710 water distribution systems. *Journal of Water Resources Planning and Management*, 138(5),
711 581-585.

712 Preis, A., and Ostfeld, A. 2008. Genetic algorithm for contaminant source characterization using
713 imperfect sensors. *Civ. Eng. Environ. Syst.*, 25(1), 29–39.

714 Qi, Z., Zheng, F., Guo, D., Maier, H. R., Zhang, T., Yu, T., and Shao, Y. 2018. Better
715 Understanding of the Capacity of Pressure Sensor Systems to Detect Pipe Burst within Water
716 Distribution Networks. *Journal of Water Resources Planning and Management*, 144(7),
717 04018035.

718 Rathi, S., Gupta, R., 2015. A simple sensor placement approach for regular monitoring and
719 contamination detection in water distribution networks. *KSCE Journal of Civil Engineering*.
720 20 (2), 1-12.

721 Soldevila, A., Blesa, J., Tornil-Sin, S., Fernandez-Canti, R.M., Puig, V., 2018. Sensor placement
722 for classifier-based leak localization in water distribution networks using hybrid feature
723 selection. *Computers & Chemical Engineering*. 108, 152e162.

724 Sweetapple, C., Fu, G., Farmani, R., & Butler, D. 2019. Exploring wastewater system performance
725 under future threats: Does enhancing resilience increase sustainability?. *Water research*, 149,
726 448-459.

- 727 Tinelli, S. et al. 2017. Sampling significant contamination events for optimal sensor placement in
728 water distribution systems. *Journal of Water Resources Planning and Management*, 143, Issue
729 9, Article number 04017058.
- 730 Tinelli, S. et al. 2018. Impact of objective function selection on optimal placement of sensors in
731 water distribution networks. *Italian Journal of Engineering Geology and Environment*, Special
732 Issue, 2018, Pages 173-178.
- 733 Van Thienen, P. 2014. Alternative strategies for optimal water quality sensor placement in drinking
734 water distribution networks. *Hydroinformatics International Conference*, New York, 2014
735 <https://academicworks.cuny.edu/cgi/viewcontent.cgi?referer=&httpsredir=1>
- 736 Wang, Qi, Michele Guidolin, Dragan Savic, and Zoran Kapelan. 2014. Two-Objective Design of
737 Benchmark Problems of a Water Distribution System Via Moeas: Towards the Best-Known
738 Approximation of the True Pareto Front. *Journal of Water Resources Planning and*
739 *Management* 141, no. 3, 04014060.
- 740 Watson, J.P., Murray, R., Hart, W.E., 2009. Formulation and optimization of robust sensor
741 placement problems for drinking water contamination warning systems. *J. Infrastruct. Syst.*
742 15 (4), 330e339.
- 743 Weickgenannt, M., Kapelan, Z., Savic, D.A. and Blokker, M. 2010. Risk-based Sensor
744 Placement for Contaminant Detection in Water Distribution Systems, *Journal of Water*
745 *Resources Planning and Management (ASCE)*, 136(6), 629-636.

746 Wu, Z.Y., Walski, T., 2006. Multi-objective optimization of sensor placement in water distribution
747 systems. In: Proc., 8th Annual Water Distribution Systems Analysis Symp. ASCE, Reston,
748 Va.

749 Yang, X., Boccelli, D.L., 2016. Model-Based Event Detection for Contaminant Warning Systems.
750 Journal of Water Resources Planning and Management 142(11), 04016048.

751 Zhao, Y., Schwartz, R., Salomons, E., Ostfeld, A., Poor, H.V., 2016. New formulation and
752 optimization methods for water sensor placement. Environmental modelling & software 76,
753 128-136.

754 Zheng, F., Du, J., Diao, K., Zhang, T., Yu, T., and Shao, Y. 2018. Investigating Effectiveness of
755 Sensor Placement Strategies in Contamination Detection within Water Distribution Systems.
756 Journal of Water Resources Planning and Management, 144(4), 06018003.

757 Zheng, F., Zecchin, A., Maier, H., and Simpson, A. 2016. Comparison of the Searching Behavior
758 of NSGA-II, SAMODE, and Borg MOEAs Applied to Water Distribution System Design
759 Problems. Journal of Water Resources Planning and Management, 142(7), 04016017.

760 Zheng, F., Zecchin, A., Newman, J., Maier, H., and Dandy, G. 2017. An Adaptive Convergence-
761 Trajectory Controlled Ant Colony Optimization Algorithm with Application to Water
762 Distribution System Design Problems. IEEE Transactions on Evolutionary Computation,
763 21(5), 773-791.